

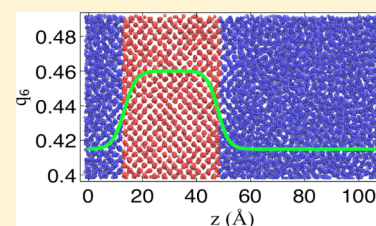
# A Comparison of the Predictive Capabilities of the Embedded-Atom Method and Modified Embedded-Atom Method Potentials for Lithium

Joseph R. Vella,<sup>†</sup> Frank H. Stillinger,<sup>‡</sup> Athanassios Z. Panagiotopoulos,<sup>†</sup> and Pablo G. Debenedetti<sup>\*,†</sup>

<sup>†</sup>Department of Chemical and Biological Engineering, and <sup>‡</sup>Department of Chemistry, Princeton University, Princeton, New Jersey 08544, United States

## S Supporting Information

**ABSTRACT:** We compare six lithium potentials by examining their ability to predict coexistence properties and liquid structure using molecular dynamics. All potentials are of the embedded-atom method type. The coexistence properties we focus on are the melting curve, vapor pressure, saturated liquid density, and vapor–liquid surface tension. For each property studied, the simulation results are compared to available experimental data in order to properly assess the accuracy of each potential. We find that the Cui second nearest-neighbor modified embedded-atom method potential is overall the most reliable potential, giving adequate agreement for most of the properties examined. For example, the zero-pressure melting point of this potential is shown to be around 443 K, while it is known from experiments to be about 454 K. This potential also gives excellent agreement for the saturated liquid densities, even though no liquid properties were used in the fitting procedure. We conclude that even though this potential is the most reliable overall, there is still room for improvement in terms of obtaining more accurate agreement for some of the properties studied, specifically the slope of the melting pressure versus temperature.



## I. INTRODUCTION

Understanding of the behavior of lithium is of fundamental importance to many applications. For example, Al–Li alloys have been the focus of much research for aerospace applications.<sup>1,2</sup> Lithium is also very important in the electrochemical industry, where several of its alloys (e.g., Li–Sn, Li–Sb, and Li–Bi) have been studied for their use as electrodes.<sup>3</sup>

A recent potential application for lithium is its use as a liquid-phase plasma-facing component (PFC) in tokamak fusion devices.<sup>4,5</sup> Liquid lithium has been one of the strongest candidates for a liquid metal PFC because of many beneficial properties such as its reactivity with hydrogen and low its atomic weight.<sup>6</sup> Several lithium alloys have also shown potential as effective PFCs, such as lithium–tin.<sup>7</sup>

The knowledge of several material properties of lithium is important for the aforementioned applications. Although there is an abundance of experimental data on pure lithium, there is a noticeable lack of data for lithium alloys, especially at the conditions of technological interest. Many of these properties are difficult to measure experimentally. Atomic-level simulations provide an attractive complement to measurements in physical property investigations. The prediction of material properties in classical simulations requires specification of an interatomic potential to describe the interaction between atoms. To study alloys using atomic-level simulations an accurate cross-potential describing the interaction between the different species within the alloy is required. However, before a cross-potential is developed one must be sure that the pure component potentials yield sufficiently accurate predictions of material properties. This is because the parameters of the pure

component potentials will be used to construct the parameters of the cross-potential. Atomic-level simulations can also provide insight into a variety of other lithium properties such as wetting of liquid lithium on solid substrates, solubilities of different species in lithium, and the location of the critical point of pure lithium.

Earlier work on the simulation of lithium has focused on the development of effective pair potentials. González Miranda and Torra<sup>8</sup> introduced pair potentials for liquid sodium and for liquid lithium near their melting points. The potential for lithium was later modified and shown to give good predictions of the specific heat, static structure factor, and self-diffusion of liquid lithium at 455 K.<sup>9</sup> Canales et al.<sup>10</sup> developed another pair potential for lithium at 470 K and showed that it gave good agreement with various properties such as the structure factor, heat capacity, diffusion coefficient, and shear viscosity. Their study was extended by looking at two types of effective pair potentials for lithium at 470 and 843 K.<sup>11</sup> These authors identified a drawback of the effective pair potential treatment of lithium. Specifically, the effective potentials were dependent on density and therefore they change at each state point. This is inconvenient for practical usage. These effective pair potentials also neglect the many-body nature of metallic bonding.

**Special Issue:** Branka M. Ladanyi Festschrift

**Received:** August 1, 2014

**Revised:** September 4, 2014

**Published:** September 5, 2014

One of the more common many-body potentials for modeling metallic systems is the embedded-atom method (EAM) developed by Daw and Baskes.<sup>12</sup> This model was first introduced to describe hydrogen embrittlement in metals.<sup>13</sup> The EAM potentials differ from interatomic potentials used in many other systems in that they contain a many-body term that is a function of an effective electron density in addition to a pair potential. The many-body term is used to capture the physics of metallic bonding. Several other many-body potentials have also been developed for the simulation of metals. They include the Finnis–Sinclair model,<sup>14</sup> the “local-volume-forces” model,<sup>15</sup> the “glue” model,<sup>16,17</sup> and the “equivalent-crystal” model.<sup>18,19</sup> All of these models are equivalent to EAM in that they also contain a many-body term that is a function of an electron density and a pair potential. The only difference between the models is the functional forms of the pair and many-body terms, parametrizations, and physical interpretations of each term.<sup>20</sup>

Lithium has also been studied using first-principles quantum mechanical simulation methods. The properties studied using those methods include structural properties,<sup>21</sup> melting,<sup>22–24</sup> and the vapor–liquid interface.<sup>25</sup> While these types of simulation studies tend to be very accurate for the properties they examined, there are limitations. First-principles simulations are significantly more computationally expensive than classical simulations. Classical simulations are able to simulate much larger systems and can access time scales that are orders of magnitude longer than first-principles studies. The calculation of several properties is facilitated by these advantages. For example, several dynamic properties rely on the calculation of autocorrelation functions and their integrals over times long enough to allow the former to vanish, or, equivalently the latter to converge. Because first-principles quantum mechanical simulation methods cannot access such long times, it is important to develop accurate empirical potentials for classical simulations.

In this work, we survey six classical potentials developed for lithium that all fall within the EAM framework. The purpose of this work is to test the accuracy and robustness of these potentials in predicting properties of lithium primarily in the liquid state. We do this by examining several properties that span a wide range of conditions; many of these properties were not used in the parametrization procedure. It should be noted that for a majority of the potentials examined, several solid-phase properties are used in the fitting procedure. Examples of solid-phase properties used in parametrization include elastic constants and surface energies. Therefore, we chose to focus on properties that were not used in the fitting procedure for most of the force fields. This allows us to examine the strengths and weaknesses of each potential and to make recommendations for future studies, including the prediction of lithium properties not yet measured experimentally. In addition, results from the present study will aid in the development of cross-potentials for binary systems. As stated earlier, because cross-potentials require accurate pure component potentials, it is important to develop an awareness of the predictive capability for different properties of pure component potentials.

This paper is organized as follows. Section II briefly reviews the different types of EAM potentials we studied. In section III, we describe the computational approaches used to compute the various properties calculated in this work. Section IV presents our results and compares the relative performance (and limitations) of each model. We conclude in section V by commenting on the significance of our results and making

recommendations on future use of the various potentials considered.

## II. MODELS

The general form of the total potential energy of a system of atoms described by the EAM formalism is given by

$$E_{\text{tot}} = \sum_i F_i(\phi_i) + \frac{1}{2} \sum_i \sum_{j \neq i} \varphi_{ij}(r_{ij}) \quad (1)$$

In the above equation  $F_i$  is called the embedding energy and is a function of the effective electron density at atom  $i$ ,  $\phi_i$ . This many-body term can be interpreted as the energy it takes to embed atom  $i$  into an effective electron density due to the surrounding atoms. The embedding energy is traditionally seen as accounting for metallic bonding. The term  $\varphi_{ij}(r_{ij})$  is a simple pair potential typically attributed to electrostatic interactions. It can be shown that the form of EAM can be derived starting from density functional theory (DFT) arguments.<sup>26</sup> However, these potentials typically require experimental data or *ab initio* calculations in order to determine specific parameters for the embedding energy, effective electron density, and pair potential. Therefore, this class of potentials is often referred to as semi-empirical. We now discuss this family of potentials by classifying them into three groups: EAM, modified embedded-atom method (MEAM), and second nearest-neighbor modified embedded-atom method (2NN MEAM). The equations and parameters for each of the potentials studied in this work are available in the Supporting Information.

**II.A. EAM Potentials.** Belashchenko and Ostrovskii<sup>27</sup> developed an EAM potential designed for liquid lithium by fitting to experimental liquid-phase pair correlation functions, atomization energy, bulk modulus, and liquid-phase densities. They found that in order to predict accurately experimental densities and energies, some of the parameters had to be temperature-dependent. Belashchenko later corrected this shortcoming by introducing a similar model<sup>28</sup> with temperature-independent parameters. This corrected model is one of the potentials examined in this paper and will be referred to as the Belashchenko 2012 model. Subsequently, Belashchenko introduced a slightly modified model<sup>29</sup> in an attempt to obtain accurate properties at high pressures. This is the second model we study in this paper and we will refer to it as the Belashchenko 2013 model.

**II.B. MEAM Potentials.** The MEAM potential model was developed as an extension of the embedded-atom method.<sup>30</sup> The general form of the potential is similar to EAM, the major difference being that the effective electron density in MEAM contains angular contributions in order to make the model applicable to materials with directional bonding. The MEAM formalism also introduced a screening function to limit the number of interactions that need to be calculated to nearest-neighbors only. The screening function defines the nearest-neighbor distance. Baskes parametrized a MEAM potential for lithium.<sup>30</sup> We examine the use of this potential and will refer to it in the text as Baskes MEAM. Yuan et al.<sup>31</sup> presented another lithium MEAM potential in which the functional form of the embedding energy was changed in order to improve the prediction of nonbulk properties of lithium, such as surface energy of the crystal-phase. This potential will be referred to as Yuan MEAM.

**II.C. 2NN MEAM Potentials.** The 2NN MEAM was developed in order to correct two shortcomings of the MEAM

potentials when simulating metals that form stable body-centered cubic (BCC) crystals.<sup>32,33</sup> It was found that for several BCC metals, the MEAM potential failed to predict the qualitative order of the surface energies of the BCC crystal. Many MEAM potentials for BCC metals predicted the surface energy of the (111) surface to be smaller than the (100) surface, which contradicts information from experiments.<sup>32</sup> Second, some MEAM potentials predicted that crystal structures other than BCC were more stable for materials where it was experimentally known that BCC was the more stable crystal structure.<sup>32</sup> This was attributed to the fact that the MEAM potentials only accounted for first nearest-neighbor interactions. As the name suggests, the 2NN MEAM formalism accounts for second nearest-neighbor interactions. This consideration changes the form of the pair potential. Two 2NN MEAM potentials for lithium can be found in the literature, one developed by Kim et al.<sup>34</sup> and one developed by Cui et al.<sup>35</sup> The first will be referred to as the Kim 2NN MEAM potential and the second will be referred to as the Cui 2NN MEAM potential. These potentials possess different values of potential parameters because different physical properties were used during the fitting procedure.

### III. METHODS

**III.A. Solid–Liquid Simulations.** The melting curve of each potential was calculated using a direct interfacial molecular dynamics technique similar to that described by Morris.<sup>36</sup> In this procedure, the first step requires that the solid and liquid phases be simulated separately. The two phases were simulated in separate boxes under NVT conditions such that the density and temperature match the experimental conditions for the zero-pressure melting point. Once each phase is equilibrated separately, they were combined with fully periodic boundary conditions, creating two interfaces. Care must be taken so that the two boxes are prepared with equal box dimensions parallel to the interface. (We designate these directions as the  $x$  and  $y$  axes, and the direction perpendicular to the interface as the  $z$  axis.) The atoms originally in the solid box were then held fixed while the atoms originally in the liquid box were relaxed in the NVT ensemble at a temperature close to melting. Once the liquid atoms were relaxed, the velocities of all the atoms were reinitialized. The velocities were randomly assigned after an initial temperature is selected. The system was then run in the NVE ensemble. If the initial temperature was set too high (relative to the coexistence temperature), the entire system melted. If it was set too low, the system froze. If the system was close enough to coexistence conditions, the pressure and temperature naturally converged to their coexistence values and solid and liquid phases coexisted in the simulation box. The system was deemed to have reached coexistence if both the solid and liquid phases were seen within the simulation box for the entire production period. Once the system was found to be at coexistence, we took the final configuration of the coexistence simulation and changed the volume and energy in order to search for other coexistence points along the melting line. As was the case for the initial coexistence simulation, the velocities were randomly assigned after an initial temperature was selected. Again, if this initial temperature was set too high (relative to the coexistence temperature) the system would melt and if it was set too low the system would freeze. Simulations were divided into a 300 ps long equilibration period and a 1000 ps long production period. It was found that the chosen length of the equilibration period

was more than sufficient for equilibration to occur: after this time the potential energy fluctuated about a constant value during the production run. During this production period the potential energy fluctuations were no more than 0.2% of the average potential energy. The temperature and pressure were calculated over the 1000 ps long production run. To get sufficient statistics, 3–5 independent runs were performed for each state point.

A molecular dynamics time step of 0.2 fs was used for the MEAM potentials while 0.1 fs was used for the EAM potentials. These values were chosen so that the total energy was adequately conserved (less than 0.02% energy drift over 1 ns) during the course of the NVE runs. A total of 13 500 atoms were used for each run in order to avoid size effects. Calculations were checked for finite size effects by repeating a few simulations with half the number of atoms. No significant differences in the results were found.

It is important to note that a common issue encountered when constructing solid–liquid interfacial simulations using the aforementioned procedure is the fact that within the solid phase, the lattice spacing in the  $x$  and  $y$  directions would not match the lattice spacing in the  $z$  direction. This would cause significant anisotropy in the diagonal components of the pressure tensor. A simple way to correct this is given by Frenkel.<sup>37</sup> The procedure is to perform bulk solid NPT simulations at coexistence conditions to get a relationship between the coexistence pressure and lattice spacing. This information is then applied to the interface simulations to adjust the  $x$  and  $y$  dimensions of the simulation box so that they match up with the lattice spacing in the  $z$  direction. Doing this ensures that there is no significant anisotropy in the diagonal components of the pressure tensor that can possibly affect the calculated melting temperature.

A snapshot of a successfully equilibrated solid–liquid interfacial simulation is shown in Figure 1. We also display the  $q_6$  order parameter<sup>38</sup> averaged over bins of width 1 Å to distinguish between the crystal and liquid phases. This parameter describes local ordering and can distinguish between phases with and without long-range order.

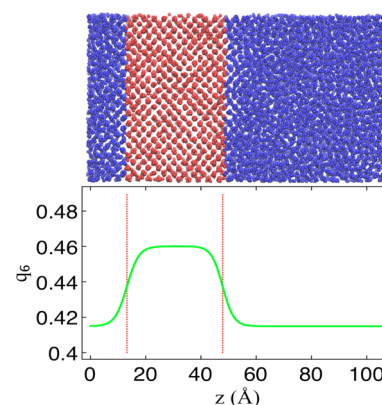


**Figure 1.** A snapshot of a solid–liquid direct interfacial simulation corresponding to the Cui 2NN MEAM potential simulation at 443 K and 0 GPa. Atoms in the solid BCC phase are red, while liquid atoms are blue. The colors are assigned based on the average  $q_6$  at each location in the  $z$  dimension. Each interface was fitted to a hyperbolic tangent function shown as the green line. The Gibbs dividing surfaces are shown as red lines. The snapshot of the solid–liquid simulation was rendered in Visual Molecular Dynamics.<sup>39</sup>

All simulations were performed using the LAMMPS package<sup>40</sup> (30-Sep-2013 version). A typical 1.3 ns simulation of 13 500 atoms using a MEAM potential took approximately 24–48 h on 16 CPU cores (2.6 GHz Sandybridge). For the EAM potentials we obtained similar performance with only 8 CPU cores.

**III.B. Vapor–Liquid Simulations.** For vapor–liquid coexistence properties, we also chose to use a direct interfacial approach. However, a slightly different procedure was used than the one for solid–liquid simulations. In this procedure, a liquid-phase simulation cell containing 6750 atoms was first equilibrated at a given temperature in the NVT ensemble. We deemed a system to be equilibrated by monitoring the potential energy and picked an equilibrium time such that the potential energy fluctuated about a constant value for a 2.5 ns production run. During this production period the potential energy fluctuations were no more than 2% of the average potential energy. We found that a 1 ns equilibration period was more than enough. Fewer atoms were chosen for these simulations because it was found that there were no finite size effects on the calculated properties at this size, and the smaller number of atoms made the computations more rapid. Once the system was equilibrated, one of the box dimensions was extended (typically about 4 times its initial amount). Again, we designate this dimension (the one that is perpendicular to the interface) as the  $z$  dimension. The system was then run under NVT conditions, whereupon it spontaneously separated into a liquid and a vapor phase.

Because we are operating within the NVT ensemble and therefore do not need to worry about energy conservation, we took a larger time step of 1 fs for all potentials. During the production run 10 000 configurations were stored and used to obtain an average density profile. We then fit each interface to the following empirical hyperbolic tangent function.<sup>41</sup>

$$\rho(z) = \frac{1}{2}(\rho^L + \rho^V) - \frac{1}{2}(\rho^L - \rho^V) \tanh[(z - z_0)/d] \quad (2)$$

The bulk liquid density is given by  $\rho^L$ , the bulk vapor density is given by  $\rho^V$ ,  $d$  is a measure of the interfacial thickness, and  $z_0$  is the position of the Gibbs dividing surface. For most simulations, when we fitted the above equation to the averaged density profile along each interface we obtained unphysical values for  $\rho^V$  (small negative numbers). However, from  $z_0$  we know the location of the Gibbs dividing surface separating the liquid and vapor phases. We used this information to calculate the bulk densities of the saturated liquid and vapor. It was found that at most a distance of 20 Å away from the Gibbs dividing surface was enough to reach the bulk liquid or bulk vapor phase. We obtained statistics on the saturated liquid and vapor densities by dividing the 2.5 ns long trajectory into 5 blocks and performing block averaging. With knowledge of the vapor density, the vapor pressure was calculated by performing bulk vapor phase simulations at the temperature and density of interest. Figure 2 shows a snapshot of the vapor–liquid simulations along with the associated density profile.

We also calculated the vapor–liquid surface tensions. We did this by using the mechanical definition,<sup>42</sup> given by eq 3. This definition relies on knowledge of the diagonal components of the pressure tensor.

$$\gamma = \frac{L_z}{2} [\langle P_{zz} \rangle - 0.5(\langle P_{xx} \rangle + \langle P_{yy} \rangle)] \quad (3)$$

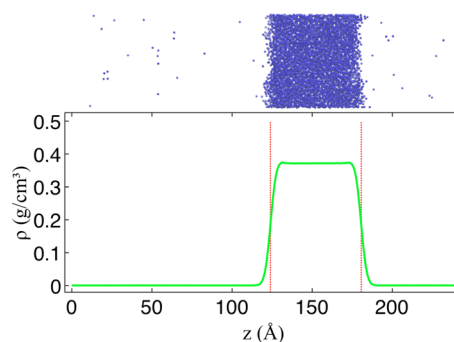


**Figure 2.** A snapshot of a vapor–liquid direct interface simulation corresponding to the Cui 2NN MEAM potential simulation at 2200 K. The graph displays the density profile shown as the green solid line. The red vertical lines correspond to the positions of the Gibbs dividing surfaces, which separate the liquid and vapor phases. The snapshot of the vapor–liquid simulation was rendered in Visual Molecular Dynamics.<sup>39</sup>

Here  $\gamma$  is the vapor–liquid surface tension,  $L_z$  is the box dimension corresponding the  $z$  direction,  $P_{xx}$ ,  $P_{yy}$ , and  $P_{zz}$  are the three diagonal components of the pressure tensor. The angled brackets denote canonical ensemble averages.

**III.C. Bulk Liquid Simulations.** We computed the radial distribution functions in the liquid-phase. For these calculations, 6750 atoms were equilibrated for 1 ns, followed by a 2.5 ns production run. We deemed a system to be equilibrated by monitoring the potential energy and picked an equilibrium time such that the potential energy fluctuated about a constant value for a 2.5 ns production run. During this production period the potential energy fluctuations were no more than 0.3% of the average potential energy. During the production run 10 000 configurations were used to calculate the radial distribution function.

## IV. RESULTS

**IV.A. Melting Curve.** The calculated melting curves for each of the potentials are presented in Figure 3, along with experimental data,<sup>43</sup> for comparison.

It is clear that none of the potentials accurately reproduce the melting curve of lithium over the pressure range considered. However, the Cui 2NN MEAM potential comes quite close to

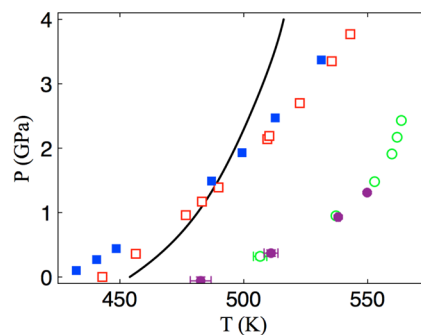


**Figure 3.** A comparison of the calculated melting curves of the different potentials. Cui 2NN MEAM (red □); Kim 2NN MEAM (blue ■); Belashchenko 2012 EAM (green ○); Belashchenko 2013 EAM (purple ●). Baskes MEAM and Yuan MEAM are not shown owing to their poor performance. Experimental results from Luedemann et al.<sup>43</sup> are shown as a black line. Simulation error bars for most of the data points are of the order of symbol size.

predicting the zero-pressure melting point. It gives a value of approximately 443 K, while experimental measurements give 454 K. This is more accurate than the calculated melting point from the first-principles study of Chen et al., which reports a calculated melting point of 434 K.<sup>22</sup> This result suggests that this potential could be promising for constructing a force field suitable for studying alloy systems. The Kim 2NN MEAM potential performs in qualitatively similar fashion to the Cui 2NN MEAM potential, however it yields a melting curve systematically lower than Cui 2NN MEAM in the pressure range studied. The two Belashchenko EAM potentials give essentially the same curve but severely overestimate the melting temperature with respect to experimental data at all values of pressure considered. Baskes MEAM and Yuan MEAM perform very poorly for the melting curve and are outside the range of the figure. We expect the Baskes MEAM to severely underestimate the melting temperature for the pressure range considered; an initial simulation showed that the liquid-phase was stable at 0 GPa and 300 K. By contrast, the Yuan MEAM is expected to overestimate the melting temperature for the pressure range considered; an initial coexistence simulation had a melting temperature of 771 K at 1 GPa.

In general, the potentials studied in this work do not accurately predict the melting curve because melting properties were not considered during their parametrization. Considering properties relevant to melting such as the enthalpy of fusion as well as both solid and liquid densities during the fitting procedure will probably yield a potential that gives better agreement with the melting curve. All of the potentials underestimate the slope of the melting curve. Insight into the underlying behavior can be found by considering the Clapeyron equation. This relation tells us that the potentials studied either underestimate the enthalpy of fusion or overestimate the volume difference between the solid and liquid phases. It is possible both cases are occurring simultaneously for one or more potential.

It should be noted that the first-principles calculations by Hernández et al.<sup>23</sup> yield very good agreement with the experimental melting curve. The first-principles study of Li et al.<sup>24</sup> also obtained good agreement. These first-principles calculations could serve as a starting point for constructing a classical potential that reproduces the melting curve better than existing MEAM and EAM potentials studied here.

**IV.B. Vapor Pressure.** Figure 4 shows the calculated vapor pressures for each potential, together with experimental data.<sup>44</sup> Similar to the melting curve, none of the potentials accurately captures the experimental data.

The models that perform best are the Cui 2NN MEAM and the Baskes MEAM force fields. Cui 2NN MEAM underestimates the vapor pressure, while Baskes MEAM overestimates it. Kim 2NN MEAM and Yuan MEAM overestimate vapor pressure more than Baskes MEAM. Finally, both Belashchenko EAM potentials severely underestimate the vapor pressure. The Belashchenko 2012 and Belashchenko 2013 vapor pressures are statistically indistinguishable, which is expected because the models only differ at high pressures.

The potentials do not accurately predict the vapor pressure curve for the same reason as for the melting curve. That is, vapor–liquid equilibrium data were not considered during the fitting of these parameters. Including vapor pressure and enthalpy of vaporization data during the fitting will most likely aid in the construction of a potential that gives better agreement with experimental vapor pressure.

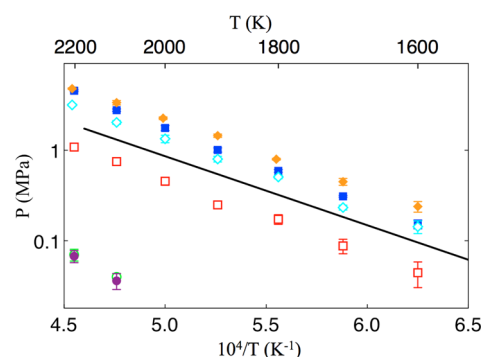


**Figure 4.** A comparison of the calculated vapor pressure for the different potentials. Cui 2NN MEAM (red  $\square$ ); Kim 2NN MEAM (blue  $\blacksquare$ ); Belashchenko 2012 EAM (green  $\circ$ ); Belashchenko 2013 EAM (purple  $\bullet$ ); Baskes MEAM (aqua  $\diamond$ ); and Yuan MEAM (orange  $\blacklozenge$ ). Experimental results from Shpil'rain et al.<sup>44</sup> are shown as a black line.

It is worthwhile to point out another interesting property captured by most of the force fields studied in this work. Figure 5 shows the density profile from a vapor–liquid interface simulation using the Cui 2NN MEAM potential at a temperature close to the melting point (460 K).

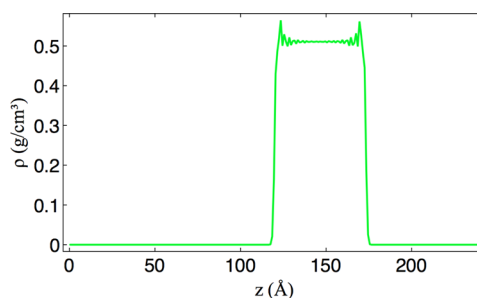


**Figure 5.** Vapor–liquid density profile of the Cui 2NN MEAM model at 460 K. Note the static density oscillations near the interface.

One can see the presence of static density oscillations near the vapor–liquid interface. The other potentials show similar behavior with the exception of Baskes MEAM which only shows one sharp rise in density at the interface. Prior theoretical and experimental studies have confirmed that the structure of vapor–liquid interface in metals displays this sort of stratification.<sup>45</sup> This shows that the three types of EAM potentials studied have the ability to reproduce the structural properties of the vapor–liquid interface of metals and can therefore prove to be a useful tool in studying this interface. This is not surprising; Rice<sup>45</sup> argues that in his simulations, the origin of the stratified structure of the interface is due to the electron density dependence of the one-body term in the pseudopotential treatment of metals. It is reasonable to assume that in the EAM formalism, the many-body embedding energy term, which also depends on an effective electron density, plays a similar role to the one-body term in the aforementioned pseudopotential treatment in giving rise to the stratified structure of the interface.

The fact that the Cui 2NN MEAM potential yields the most accurate values for vapor pressures compared to the other potentials studied in this work and also captures the qualitative behavior of the vapor–liquid interface suggests that the 2NN

MEAM class of potentials can be used to study vapor–liquid equilibrium in other metals if parametrized correctly.

**IV.C. Saturated Liquid Densities.** Figure 6 shows calculated saturated liquid densities. We should note that we

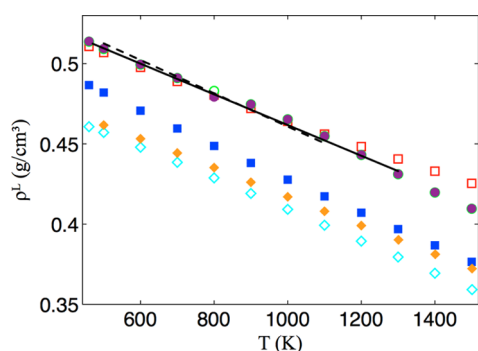


**Figure 6.** A comparison of calculated saturated liquid densities for the different potentials. Cui 2NN MEAM (red  $\square$ ); Kim 2NN MEAM (blue  $\blacksquare$ ); Belashchenko 2012 EAM (green  $\circ$ ); Belashchenko 2013 EAM (purple  $\bullet$ ); Baskes MEAM (aqua  $\diamond$ ); and Yuan MEAM (orange  $\blacklozenge$ ). Experimental results from Yakimovich et al.<sup>46</sup> are shown as a solid black line, and from Novikov et al.<sup>47</sup> as a dashed black line. Simulation error bars are smaller than the symbol size.

compare this to experimental data<sup>46,47</sup> for liquid lithium at atmospheric pressure rather than at coexistence. However, due to the fact that the vapor pressure of lithium is less than 1 MPa at the temperatures considered, and that liquids are incompressible, we believe this is still a valid comparison.

Both Belashchenko EAM potentials give excellent agreement with experimental data. Again, they give essentially the same predictions. This is expected, since liquid densities were properties used during the fitting procedure for these potentials. Cui 2NN MEAM also gives good agreement; however, it starts to show a deviation at higher temperatures. The other three potentials underestimate the liquid densities. The performance of the Cui 2NN MEAM is encouraging as no liquid properties were used during the fitting procedure.

**IV.D. Vapor–Liquid Surface Tension.** The results of the vapor–liquid surface tension calculations are shown in Figure 7. The Belashchenko EAM potentials provide the best agreement with experiment<sup>46,48</sup> although they overestimate this property at any given temperature. Once again, they both give the same

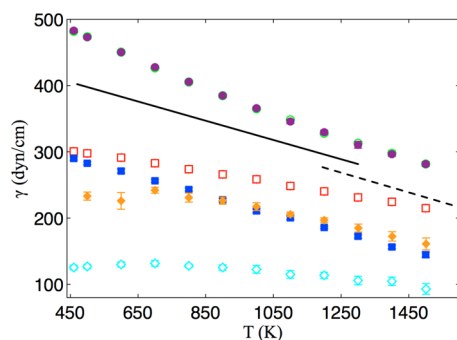


**Figure 7.** A comparison of the vapor–liquid surface tension for the different potentials. Cui 2NN MEAM (red  $\square$ ); Kim 2NN MEAM (blue  $\blacksquare$ ); Belashchenko 2012 EAM (green  $\circ$ ); Belashchenko 2013 EAM (purple  $\bullet$ ); Baskes MEAM (aqua  $\diamond$ ); and Yuan MEAM (orange  $\blacklozenge$ ). Experimental results from Yakimovich et al.<sup>46</sup> are shown as a solid black line and from Bohdansky et al.<sup>48</sup> as a dashed black line.

predictions. The other four potentials underestimate the values for surface tension, with the Cui 2NN MEAM being the closest to the experiments. All of the potentials provide surface tension calculations that are consistent with the respective vapor pressure calculations, with the exception of the Baskes MEAM force field. That is, a potential that yields low vapor pressure will give high vapor–liquid surface tension. Again, improvement in the models' prediction of the vapor–liquid surface tension could be obtained by using vapor–liquid coexistence data in the fitting procedure.

**IV.E. Liquid Radial Distribution Function.** Figure 8 displays the radial distribution functions of liquid lithium at two

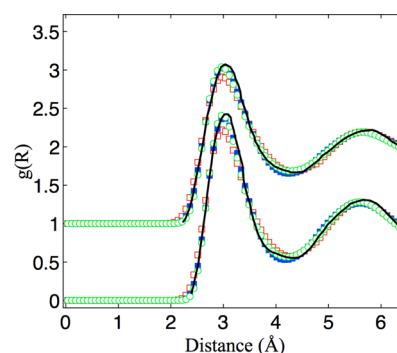


**Figure 8.** A comparison of the radial distribution function of liquid lithium for the different potentials at 470 and 725 K. The curves at 725 K are shifted up for ease of comparison: Cui 2NN MEAM (red  $\square$ ); Kim 2NN MEAM (blue  $\blacksquare$ ); Belashchenko 2012 EAM (green  $\circ$ ). The results from the Belashchenko 2013 EAM force field are statistically indistinguishable from the Belashchenko 2012 EAM force field and are therefore not shown for clarity. Baskes MEAM and Yuan MEAM are excluded due to their poor agreement. Experimental results from Olbrich et al.<sup>49</sup> are shown as solid black lines.

different state points ( $T = 470$  K,  $\rho = 0.5134$  g/cm<sup>3</sup> and  $T = 725$  K,  $\rho = 0.4910$  g/cm<sup>3</sup>). The Belashchenko EAM potentials agree well with experimental data.<sup>49</sup> This is expected as these potentials were fitted to radial distribution functions. The Kim 2NN MEAM and Cui 2NN MEAM potentials also perform well, with the latter doing slightly worse due to underestimating the first peak. Baskes MEAM and Yuan MEAM are not displayed in Figure 8 because both potentials overestimate the value of the first peak. However, they can be found in the Supporting Information. In a similar manner to the saturated liquid densities, the performance of the Cui 2NN MEAM potential (and the Kim 2NN MEAM potential in this case) at predicting liquid-phase radial distribution functions is encouraging as no liquid data were used during the fitting procedure.

## V. CONCLUDING REMARKS

In this work, we examined six interatomic potentials available in the literature, all designed to simulate lithium. These potentials can be considered as part of the EAM framework, and can be further divided into three subclasses: EAM potentials (Belashchenko 2012 and Belashchenko 2013), MEAM potentials (Baskes MEAM and Yuan MEAM), and 2NN MEAM (Cui 2NN MEAM and Kim 2NN MEAM). Using molecular dynamics simulations, we tested each potential's ability to predict several properties of lithium. The properties considered in this work are the melting curve, vapor pressure,

saturated liquid densities, vapor–liquid surface tension, and liquid-phase radial distribution functions.

For the melting curve, the Cui 2NN MEAM potential performs the best. Although it does not predict accurately the melting curve over the entire pressure range considered, it provides a good prediction of the zero-pressure melting point, giving a value of 443 K. This is close to the experimental value of 454 K and slightly more accurate than the first-principles study of Chen et al.<sup>22</sup> which reports a value of 434 K. Therefore, this potential will be useful if one wants to construct cross-potentials for lithium alloys that accurately reproduce the binary phase diagrams. However, the first-principles studies of Hernández et al.<sup>23</sup> and Li et al.<sup>24</sup> give better agreement with the melting curve compared to any of the potentials studied in this work.

For the vapor pressure, the Cui 2NN MEAM performs the best, with the Baskes MEAM performing second best. Cui 2NN MEAM underestimates the vapor pressure while Baskes overestimates it. It was also shown that the Cui 2NN MEAM exhibits static density oscillations at the vapor–liquid interface, expected in metallic systems, which agrees with a previous first-principles study<sup>25</sup> and with experiment. We note that the other force fields, with the exception of the Baskes MEAM potential, also exhibit this behavior. As stated earlier, this illustrates that the three types of EAM potentials studied in this work could be useful in studying vapor–liquid equilibrium properties of metals. This could be very useful in estimating the critical points of metals. The critical region of many metals occurs at high temperatures and is difficult to observe experimentally. Previous studies often rely on theoretical arguments to estimate the location of the critical point.<sup>50</sup> Therefore, reliable potentials could help provide insight into the location of critical points.

The Belashchenko EAM potentials provide excellent agreement with experimental data for saturated liquid densities. This is expected, as liquid lithium densities were used in the fitting procedure for these potentials. It is more surprising to see that the Cui 2NN MEAM yields good predictions since no liquid data were used in fitting. This illustrates the robustness of the Cui 2NN MEAM force field.

The Belashchenko EAM potentials also provide the best agreement with vapor–liquid surface tensions, although they overestimate the actual values. After these potentials the Cui 2NN MEAM gives the best agreement, although it underestimates this property. The other potentials underestimate the vapor–liquid surface tension even more than the Cui 2NN MEAM.

For liquid-phase radial distribution functions the Belashchenko EAM potentials give the best agreement with experiment. Again, this is because those functions were considered during the fitting procedure for these potentials. The good agreement of both the Kim and Cui 2NN MEAM potentials with experimental data is surprising, since these force fields were not parametrized with liquid-phase data. The Cui 2NN MEAM potential performs slightly worse due to underestimating the first radial distribution function peak. These classical potentials essentially do as well as first-principles methods<sup>21,22</sup> with respect to the liquid-phase radial distribution function.

From the present study, we can conclude that the Cui 2NN MEAM potential is the most robust among the lithium potentials examined. This is because it seems to perform the best or at least adequately in most properties studied over a fairly broad range of conditions compared to the other force

fields studied in this work. This potential also performs well for some properties not considered during its parameter fitting. Therefore, this potential appears to be the best choice to be used in further studies of lithium, or at least as a starting point in the construction of new and improved potentials.

This study also allows us to make a statement about the three types of models we studied. Not surprisingly, the model that seems to be the most robust falls within the 2NN MEAM class of potentials, which is representative of the most recent improvement of EAM potentials. This is perhaps a good indication that the 2NN MEAM formalism is a good framework in predicting properties of metals. The 2NN MEAM potential has been shown to be particularly well-suited for predicting properties of BCC metals (such as lithium), and we have shown that it also has the ability to capture the structure of the vapor–liquid interface. Future work will focus on the prediction of transport properties of lithium, such as the self-diffusion coefficient and viscosity, using the Cui 2NN MEAM potential. This potential will also be considered when constructing cross-potentials for binary systems. These include cross-potentials for lithium–tin alloys and hydrogen/deuterium–lithium mixtures. The development of 2NN MEAM cross-potentials for binary lithium systems has been done for Mg–Li<sup>34</sup> and for Li–Si<sup>51</sup> alloys. Therefore, a similar approach can be taken for other binary systems of interest.

This study illustrates that there is still room for improvement in the development of an EAM potential for lithium. To obtain a better prediction of the various properties we studied, one can refit the various models by including different properties in the fitting procedure. For example, one could include enthalpies of fusion to get better agreement with the melting curve, and enthalpy of vaporization for vapor pressures. Caution should be used if one wants to adjust the parameters of an existing model because the new model may give worse predictions of the material properties to which it was originally fitted. It would also be worthwhile to explore if an adjustment on the form of the model is able to more accurately reproduce the properties of lithium studied in this work. One possible adjustment could be the inclusion of third nearest-neighbor interactions in the development of the force field.

## ■ ASSOCIATED CONTENT

### 📄 Supporting Information

Raw data and estimated uncertainties as well as liquid-phase radial distribution functions for Baskes MEAM and Yuan MEAM which were excluded from Figure 8; the functional form and parameters for each of the lithium potentials studied in this work. This material is available free of charge via the Internet at <http://pubs.acs.org>.

## ■ AUTHOR INFORMATION

### Corresponding Author

\*E-mail: [pdebene@princeton.edu](mailto:pdebene@princeton.edu).

### Notes

The authors declare no competing financial interest.

## ■ ACKNOWLEDGMENTS

The authors thank the Office of Fusion Energy Science, U.S. Department of Energy, which provided support for this work under Award DE-SC0008598. The authors thank Zhiwei Cui, Jianmin Qu, Byeong-Joo Lee, David Belashchenko, Kunio Takahashi, and Michael Baskes for their help in implementing

their potentials in LAMMPS. The authors also thank Gregory Wagner for his help in editing code to account for functional forms not implemented in LAMMPS and Arash Nikoubashman for providing code to calculate bond order parameters.

## REFERENCES

- (1) Starke, E. A., Jr.; Staley, J. T. Application of Modern Aluminum Alloys to Aircraft. *Prog. Aerospace Sci.* **1996**, *32*, 131–172.
- (2) Dursun, T.; Soutis, C. Recent Developments in Advanced Aircraft Aluminium Alloys. *Mater. Des.* **2014**, *56*, 862–871.
- (3) Wang, J.; Raistrick, I. D.; Huggins, R. A. Behavior of Some Binary Lithium Alloys as Negative Electrodes in Organic Solvent-Based Electrolytes. *J. Electrochem. Soc.* **1986**, *133*, 457–460.
- (4) Hassanein, A.; Allain, J. P.; Insepov, Z.; Konkashbaev, I. Plasma/Liquid–Metal Interactions during Tokamak Operation. *Fusion Sci. Technol.* **2005**, *47*, 686–697.
- (5) Coenen, J. W.; De Temmerman, G.; Federici, G.; Philipps, V.; Sergienko, G.; Strohmayer, G.; Terra, A.; Unterberg, B.; Wegener, T.; Vanden Bekerom, D. C. M. Liquid Metals as Alternative Solution for the Power Exhaust of Future Fusion Devices: Status and Perspective. *Phys. Scr.* **2014**, *2014*, 014037.
- (6) Majeski, R. Liquid Metal Walls, Lithium and Low Recycling Boundary Conditions in Tokamaks. *AIP Conf. Proc.* **2010**, *1237*, 122–137.
- (7) Allain, J. P.; Ruzic, D. N.; Hendricks, M. R. D, He, and Li Sputtering of Liquid Eutectic Sn–Li. *J. Nucl. Mater.* **2001**, *290–293*, 33–37.
- (8) González Miranda, J. M.; Torra, V. The Effect of the Born-Mater Core on the Properties of Liquid Lithium and Sodium at their Melting Points. *Phys. Lett. A* **1984**, *103*, 126–128.
- (9) González Miranda, J. M. An Effective Pair Potential for Liquid Lithium at 455 K. *Phys. Lett. A* **1985**, *108*, 35–38.
- (10) Canales, M.; Padroó, J. E.; González, L. E.; Giró, A. Molecular Dynamics Simulation of Liquid Lithium. *J. Phys.: Condens. Matter* **1993**, *5*, 3095–3102.
- (11) Canales, M.; González, L. E.; Padroó, J. E. Computer Simulation Study of Liquid Lithium at 470 and 843 K. *Phys. Rev. E* **1994**, *50*, 3656.
- (12) Daw, M. S.; Baskes, M. I. Embedded-Atom Method: Derivation and Application to Impurities, Surfaces, and Other Defects in Metals. *Phys. Rev. B* **1983**, *29*, 6443–6453.
- (13) Daw, M. S.; Baskes, M. I. Semiempirical, Quantum Mechanical Calculation of Hydrogen Embrittlement in Metals. *Phys. Rev. Lett.* **1983**, *50*, 1285–1288.
- (14) Finnis, M. W.; Sinclair, J. E. A Simple Empirical N-Body Potential for Transition Metals. *Philos. Mag. A* **1984**, *50*, 45–55.
- (15) Chen, S. P.; Voter, A. F.; Sroloitz, D. J. Oscillatory Surface Relaxations in Ni, Al, and Their Ordered Alloys. *Phys. Rev. Lett.* **1986**, *57*, 1308–1311.
- (16) Erolessi, F.; Parrinello, M.; Tosatti, E. Au(100) Reconstruction in the Glue Model. *Surf. Sci.* **1986**, *177*, 314–328.
- (17) Erolessi, F.; Tosatti, E.; Parrinello, M. Au(100) Surface Reconstruction. *Phys. Rev. Lett.* **1986**, *57*, 719–722.
- (18) Smith, J. R.; Banerjee, A. New Approach to Calculation of Total Energies of Solids with Defects: Surface-Energy Anisotropies. *Phys. Rev. Lett.* **1987**, *59*, 2451–2454.
- (19) Smith, J. R.; Banerjee, A. Equivalent-Crystal Theory of Oscillatory Surface Relaxation. *Phys. Rev. B* **1988**, *37*, 10411–10414.
- (20) Daw, M. S.; Foiles, S. M.; Baskes, M. I. The Embedded-Atom Method: A Review of Theory and Applications. *Mater. Sci. Rep.* **1988**, *9*, 251–310.
- (21) Wentzcovitch, R. M.; Martins, J. M. First Principles Molecular Dynamics of Li: Test of a New Algorithm. *Solid State Commun.* **1991**, *78*, 831–834.
- (22) Chen, M.; Hung, L.; Huang, C.; Xia, J.; Carter, E. A. The Melting Point of Lithium: An Orbital-Free First-Principles Molecular Dynamics Study. *Mol. Phys.* **2013**, *111*, 3448–3456.
- (23) Hernández, E. R.; Rodríguez-Prieto, A.; Bergara, A.; Alfé, D. First-Principles Simulations of Lithium Melting: Stability of the BCC Phase Close to Melting. *Phys. Rev. Lett.* **2010**, *104*, 185701.
- (24) Li, D. F.; Zhang, P.; Yan, J.; Liu, H. Y. Melting Curve of Lithium from Quantum Molecular-Dynamics Simulations. *Europhys. Lett.* **2011**, *95*, S6004.
- (25) González, D. J.; González, L. E.; Stott, M. J. Surface Structure of Liquid Li and Na: An *Ab Initio* Molecular Dynamics Study. *Phys. Rev. Lett.* **2004**, *92*, 085501.
- (26) Daw, M. S. Model of Metallic Cohesion: The Embedded-Atom Method. *Phys. Rev. B* **1988**, *39*, 7441–7452.
- (27) Belashchenko, D. K.; Ostrovskii, O. I. Application of the Embedded Atom Model to Liquid Metals: Liquid Lithium. *High Temp.* **2009**, *47*, 231–237.
- (28) Belashchenko, D. K. Electron Contribution to Energy of Alkali Metals in the Scheme of an Embedded Atom Model. *High Temp.* **2012**, *50*, 331–339.
- (29) Belashchenko, D. K. Impact Compression of Alkali Metals: Computer Aided Simulation. *High Temp.* **2013**, *51*, 626–639.
- (30) Baskes, M. I. Modified Embedded-Atom Potentials for Cubic Materials and Impurities. *Phys. Rev. B* **1992**, *46*, 2727–2742.
- (31) Yuan, X.; Takahashi, K.; Yin, Y.; Onzawa, T. Development of Modified Embedded Atom Method for a BCC Metal: Lithium. *Model. Simul. Mater. Sci. Eng.* **2003**, *11*, 447–456.
- (32) Lee, B.; Baskes, M. I. Second Nearest-Neighbor Modified Embedded-Atom-Method Potential. *Phys. Rev. B* **2000**, *62*, 8564–8567.
- (33) Lee, B.; Baskes, M. I.; Kim, H.; Cho, Y. K. Second Nearest-Neighbor Modified Embedded Atom Method Potentials for BCC Transition Metals. *Phys. Rev. B* **2001**, *64*, 184102.
- (34) Kim, Y.; Jung, I.; Lee, B. Atomistic Modeling of Pure Li and Mg–Li System. *Model. Simul. Mater. Sci. Eng.* **2012**, *20*, 035005.
- (35) Cui, Z.; Gao, F.; Cui, Z.; Qu, J. Developing a Second Nearest-Neighbor Modified Embedded Atom Method Interatomic Potential for Lithium. *Model. Simul. Mater. Sci. Eng.* **2012**, *20*, 015014.
- (36) Morris, J. R. The Melting Lines of Model Systems Calculated From Coexistence Simulations. *J. Chem. Phys.* **2002**, *116*, 9352–9358.
- (37) Frenkel, D. Simulations: The Dark Side. *Eur. Phys. J. Plus* **2013**, *10*.
- (38) Steinhardt, P. J.; Nelson, D. R.; Ronchetti, M. Bond-Orientational Order in Liquids and Glasses. *Phys. Rev. B* **1983**, *28*, 784–805.
- (39) Humphrey, W.; Dalke, A.; Schulten, K. VMD—Visual Molecular Dynamics. *J. Mol. Graphics* **1996**, *14*, 33–38.
- (40) Plimpton, S. Fast Parallel Algorithms for Short-Range Molecular Dynamics. *J. Comput. Phys.* **1995**, *117*, 1–19, <http://lammps.sandia.gov>.
- (41) Chapela, G. A.; Saville, G.; Thompson, S. M.; Rowlinson, J. S. Computer Simulations of a Gas-Liquid Surface Part 1. *J. Chem. Soc., Faraday Trans. 2* **1977**, *73*, 1133–1144.
- (42) Rowlinson, J. S.; Widom, B. *Molecular Theory of Capillarity*; Clarendon Press: Oxford, Oxfordshire, 1982.
- (43) Luedemann, H. D.; Kennedy, G. C. Melting Curves of Lithium, Sodium, Potassium and Rubidium to 80 Kilobars. *J. Geophys. Res.* **1968**, *73*, 2795–2805.
- (44) Shpil’rain, E. E.; Belova, A. M. Experimental Measurement of the Pressure of Saturated Lithium. *Teplofizika Vysokikh Temperatur* **1968**, *6*, 342–343.
- (45) Rice, S. A. Structure of the Liquid-Vapor Interfaces of Metals and Binary Alloys. *J. Non-Cryst. Solids* **1996**, *205–207*, 755–761.
- (46) Yakimovich, K. A.; Mozgovoii, A. G. Experimental Investigation of the Density and Surface Tension of Molten Lithium at Temperatures up to 1300K. *High Temp.* **2000**, *4*, 657–659.
- (47) Novikov, I. I.; Trelin, Y. S.; Tsyganova, T. A. Experimental Data on the Speed of Sound in Lithium up to 1100 K. *Teplofiz. Vys. Temp.* **1969**, *7*, 1220–1221.
- (48) Bohdansky, J.; Schins, H. E. J. The Surface Tension of the Alkali Metals. *J. Inorg. Nucl. Chem.* **1967**, *29*, 2173–2179.



- (49) Olbrich, H.; Ruppertsberg, H.; Steeb, S. Experimental-Determination of the Form and Structure Factor of Molten Lithium. *Z. Naturforsch., A* **1983**, *38*, 1328–1336.
- (50) Schröer, W.; Pottlacher, G. Estimation of Critical Data and Phase Diagrams of Pure Molten Metals. *High Temp.-High Press.* **2014**, *43*, 201–215.
- (51) Cui, Z.; Gao, F.; Cui, Z.; Qu, J. A Second Nearest-Neighbor Embedded Atom Method Interatomic Potential for Li-Si Alloys. *J. Power Sources* **2012**, *207*, 150–159.